View metadata, citation and similar papers at core.ac.uk

brought to you by CORE

provided by Infoscience - École polytechnique fédérale de Lausanne

nature materials

ARTICLES

PUBLISHED ONLINE: 23 JUNE 2013 | DOI: 10.1038/NMAT3687

Mobility engineering and a metal–insulator transition in monolayer MoS_2

Branimir Radisavljevic and Andras Kis*

Two-dimensional (2D) materials are a new class of materials with interesting physical properties and applications ranging from nanoelectronics to sensing and photonics. In addition to graphene, the most studied 2D material, monolayers of other layered materials such as semiconducting dichalcogenides MoS_2 or WSe_2 are gaining in importance as promising channel materials for field-effect transistors (FETs). The presence of a direct bandgap in monolayer MoS_2 due to quantum-mechanical confinement allows room-temperature FETs with an on/off ratio exceeding 10^8. The presence of high-κ dielectrics in these devices enhanced their mobility, but the mechanisms are not well understood. Here, we report on electrical transport measurements on MoS_2 FETs in different dielectric configurations. The dependence of mobility on temperature shows clear evidence of the strong suppression of charged-impurity scattering in dual-gate devices with a top-gate dielectric. At the same time, phonon scattering shows a weaker than expected temperature dependence. High levels of doping achieved in dual-gate devices also allow the observation of a metal–insulator transition in monolayer MoS_2 due to strong electron–electron interactions. Our work opens up the way to further improvements in 2D semiconductor performance and introduces MoS_2 as an interesting system for studying correlation effects in mesoscopic systems.

Molybdenum disulphide (MoS_2) is a layered transition-metal dichalcogenide semiconductor[1] with potential applications that could complement those of graphene. As neighbouring layers in transition-metal dichalcogenide crystals are weakly bound through van der Waals interactions, single atomic crystals composed of one or several layers can be extracted using the micromechanical cleavage technique[2] or liquid-phase exfoliation[3,4]. Large-area MoS_2 can also be grown using techniques such as chemical vapour deposition[5,6]. The strong covalent bonding between metal and chalcogenide atoms results in a high mechanical strength[7] of MoS_2 membranes[8] and electrical breakdown current densities at least 50 times higher than in copper[9]. In contrast to graphene, the presence of a bandgap in monolayer MoS_2 and other semiconducting dichalcogenides allows the fabrication of transistors that can be turned off and used as switches[10]. Logic circuits[11] and amplifiers[12] with high gain based on monolayer MoS_2 have also been demonstrated, and superconductivity in 20-nm-thick MoS_2 was achieved at high electron concentrations using ionic-liquid gating[13].

Monolayer MoS_2 has electronic and optical properties that are fundamentally different from those of thicker layers owing to quantum-mechanical confinement[14,15]. Bulk MoS_2 is an indirect gap semiconductor whereas single-layer MoS_2 has a direct gap[14–17]. The lack of inversion symmetry results in strong coupling of spin and valley degrees of freedom[18–20] and could be used in devices based on the valley Hall effect[21]. The atomic-scale thickness (6.5 Å) of monolayer MoS_2, smaller than the screening length, also allows a large degree of electrostatic control over the electrical conductivity. Together with the absence of dangling bonds, this would allow transistors based on monolayer MoS_2 to outperform silicon transistors at the scaling limit[22,23].

Previous measurements have shown that the room-temperature mobility of bulk MoS_2 is in the 200–500 $cm^2 V^{-1} s^{-1}$ range and is limited by phonon scattering[24]. Exfoliation of single layers onto SiO_2 results in a decrease of mobility down to the 0.1–10 $cm^2 V^{-1} s^{-1}$ range[2,10]. Charge traps[25] present at the interface between the substrate and the MoS_2 layer have recently been proposed as the dominant cause for such low room-temperature mobility in MoS_2 devices. Understanding the origin of this mobility degradation and finding a way to restore the mobility to bulk values or even further enhance it would allow us to unlock the full technological potential of this material.

The encapsulation of monolayer MoS_2 in a high-κ dielectric environment[26] was shown to result in an increase of the room-temperature mobility[10]. This was tentatively assigned to reduced Coulomb scattering due to the high-κ dielectric environment[26] and possible modification of phonon dispersion in MoS_2 monolayers. An increase of mobility with the dielectric deposition, similar to that in monolayers, was also observed in multilayer samples[27,28] and monolayer samples with polymer gating[29]. Previous mobility estimates for monolayer MoS_2 are however based on two-contact measurements and lack the information on their temperature dependence. More accurate measurements are needed to gain a better understanding of the various mechanisms that could limit the mobility in monolayer MoS_2. In the phonon-limited high-temperature part, the mobility is expected to follow a $\mu \sim T^{-\gamma}$ temperature dependence with $\gamma = 1.69$ and mobility reaching a room-temperature value $\sim$410 $cm^2 V^{-1} s^{-1}$ according to first-principles calculations[30]. The deposition of a top-gate dielectric is expected to mechanically quench the homopolar phonon mode and reduce the coefficient γ to 1.52.

Here, we report on mobility measurements in monolayer MoS_2 based on the Hall effect. This allows us to remove the effect of contact resistance and also directly measure the gate-modulated charge density and gate capacitance necessary for the accurate measurements of the field-effect mobility. Our devices are FETs in single- and dual-gate configurations shown in Fig. 1. Degenerately doped Si wafers covered with 270 nm thermally grown SiO_2 serve as the substrate and back-gate. MoS_2 flakes are shaped into Hall bars using oxygen plasma etching. A 30-nm-thick HfO_2 layer deposited

Electrical Engineering Institute, Ecole Polytechnique Federale de Lausanne (EPFL), CH-1015 Lausanne, Switzerland. *e-mail: andras.kis@epfl.ch

© 2013 Macmillan Publishers Limited. All rights reserved.

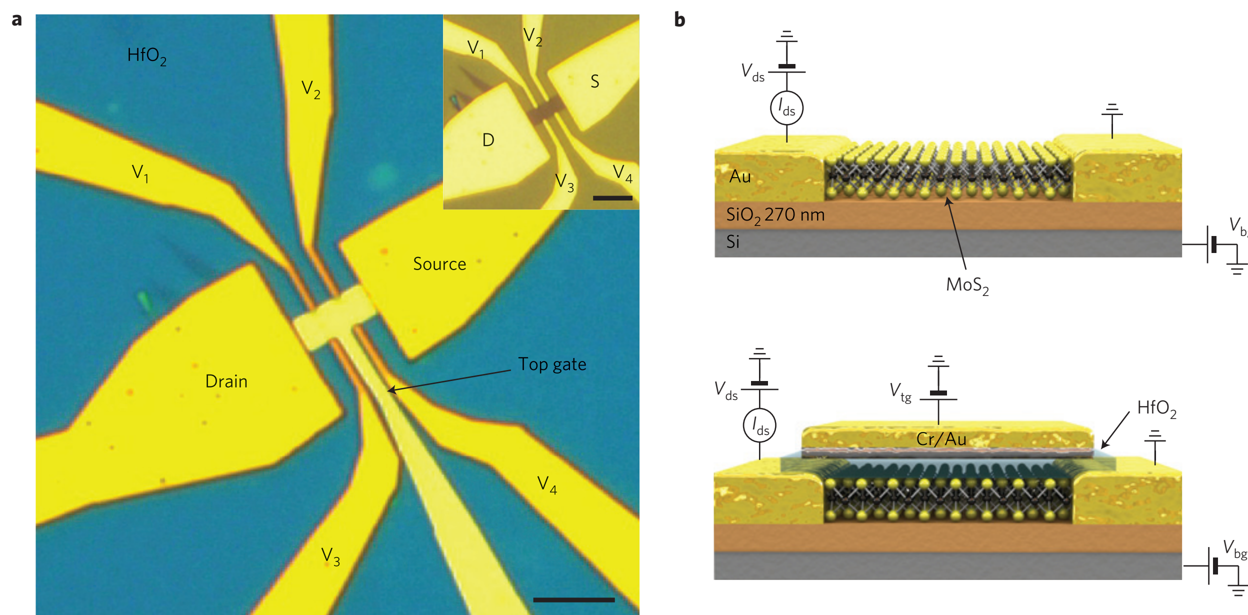

Figure 1 | Fabrication of single-gated and dual-gated MoS_2 devices. a, Optical image of the MoS_2 dual-gated device used in our measurements. The inset shows the single-gate version of the same device before ALD deposition of HfO_2 and top-gate electrode fabrication. Scale bars, 5 μm. **b**, Cross-sectional views of devices based on single-layer MoS_2 in a single-gate (top) and dual-gate (bottom) configuration. Gold leads are used for the source, drain and voltage probes (V_1, V_2, V_3 and V_4). Voltage probes have been omitted from the drawing. The silicon substrate, covered with a 270-nm-thick SiO_2 layer was used as the back gate. The top-gate dielectric is a 30-nm-thick HfO_2 layer.

by atomic layer deposition (ALD) forms the top-gate dielectric. The optical image of one of our top-gated devices is shown in Fig. 1a.

We have performed measurements on multiple devices in single- and dual-gate configurations (Fig. 1b; for more details on devices see Supplementary Table S1). By using the top gate we can induce stronger electrostatic doping of our monolayer MoS_2 owing to the higher dielectric constant and smaller thickness of the HfO_2 layer ($\varepsilon_{r2} \sim 19$, d_{ox2} $(HfO_2) = 30$ nm) compared with the bottom-gate SiO_2 ($\varepsilon_{r1} \sim 3.9$, d_{ox1} $(SiO_2) = 270$ nm). For both types of device, we measure the four-probe conductance defined as $G = I_{ds}/(V_1 - V_2)$, where I_{ds} is the drain current and $V_1 - V_2$ is the measured voltage difference between the voltage probes.

A typical conductance, G, dependence on the gate voltage for a single-gate device is shown in Fig. 2a, measured up to the back-gate voltage $V_{bg} = 40$ V that corresponds to a charge concentration of $n_{2D} \sim 3.6 \times 10^{12}$ cm^{-2} calculated using the parallel-plate capacitor model, with $n_{2D} = C_{ox1} \Delta V_{bg}/e$, where $C_{ox1} = \varepsilon_0 \varepsilon_{r1}/d_{ox1}$, $\varepsilon_0 = 8.85 \times 10^{-12}$ F m^{-1}, $e = 1.602 \times 10^{-19}$ C is the elementary charge and $\Delta V_{bg} = V_{bg} - V_{bg,th}$. The value of threshold voltage $V_{bg,th}$ varies for each device and is close to its pinch-off voltage estimated from the conductance curves. We find that the temperature variation of G in a single-gate monolayer device (Fig. 2b), in the high-temperature regime (80 K $\leq T \leq$ 280 K), can be modelled with thermally activated transport:

$$G = G_0(T) e^{-E_a/k_B T}$$

where E_a is the activation energy, k_B is the Boltzmann constant and $G_0(T)$ is the temperature-dependent parameter extracted from the fitting curves. The good agreement of the data with the activation transport model at higher temperatures is suggestive of charge transport that is thermally activated. At temperatures $T \leq 80$ K we observe that the variation of G weakens for almost all V_{bg} values. This can be explained with hopping through localized states becoming dominant at lower temperatures[25], driving the system into a strongly localized regime. The inset of Fig. 2a shows double sweeps of I_{ds}–V_{ds} characteristics for several temperatures at $V_{bg} = 30$ V with negligible hysteresis for all temperatures and nonlinear behaviour vanishing completely for temperatures above 40 K, excluding the possibility of the contact resistance or Schottky barrier influencing the mobility extraction. Figure 2c shows the temperature dependence of mobility in this device. Mobility is extracted from the conductance curves in the 30–40 V range of back-gate voltage V_{bg}, using the expression for field-effect mobility $\mu = [dG/dV_{bg}] \times [L_{12}/(WC_{ox1})]$. The temperature dependence is characterized by a peak at ~200 K. Below 200 K, we observe a decrease of the mobility as the temperature is lowered down to 4 K. This behaviour is consistent with mobility limited by scattering from charged impurities[31]. Increasing the temperature above 200 K also results in a strong decrease of the mobility from the peak value of 18 cm^2 V s^{-1}, related to electron–phonon scattering that becomes the dominant scattering mechanism at higher temperatures[30]. We fit this part of the curve with the generic temperature dependence of the mobility $\mu \sim T^{-\gamma}$, where the exponent depends on the dominant phonon scattering mechanism. From the fit we find the value of $\gamma \approx 1.4$, in good agreement with theoretical predictions for monolayer MoS_2 ($\gamma \approx 1.69$; ref. 30).

We now examine dual-gated devices. Figure 3a shows a typical top-gating dependence of the four-contact G and sheet conductivity σ, defined as $\sigma = GL_{12}/W$ with $L_{12} = 1.55$ μm and $W = 1.9$ μm being the distance between the voltage probes and the device width, respectively. The use of the top gate allows a higher degree of doping, up to $n_{2D} \sim 3.6 \times 10^{13}$ cm^{-2} (Supplementary Fig. S1), much higher than typical values for single-gated devices ($n_{2D} \sim 4 \times 10^{12}$ cm^{-2}). We observe here an insulating behaviour that persists until $V_{tg} = 2.2$ V. At this point, corresponding to $n_{2D} \sim 1 \times 10^{13}$ cm^{-2} (as measured from the Hall effect), monolayer MoS_2 enters a metallic state and the associated metal–insulator transition[32] (MIT) is observed, the first of its kind in a 2D semiconductor (Fig. 3a). This transition manifests itself as a crossing-over between conductance versus gate voltage curves acquired at different temperatures, indicating two different regimes. For gate voltages corresponding to charge densities smaller than $n_{2D} \sim 1 \times 10^{13}$ cm^{-2}, monolayer MoS_2 behaves as a classical semiconductor with conductance decreasing

© 2013 Macmillan Publishers Limited. All rights reserved.

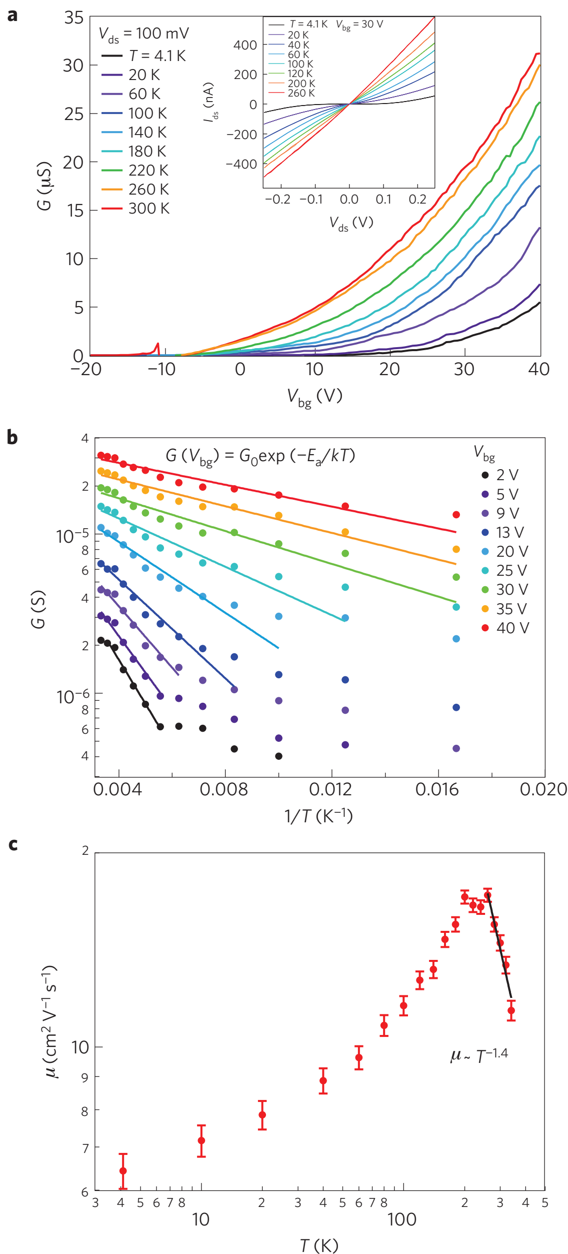

Figure 2 | Electron transport in single-gate monolayer MoS_2 supported on SiO_2. a, G as a function of V_{bg} for a single-gate monolayer MoS_2 device acquired at different temperatures. The inset shows double sweeps of I_{ds}–V_{ds} characteristics for several temperatures at $V_{bg} = 30$ V with negligible hysteresis for all temperatures. **b**, Arrhenius plot of G for different values of V_{bg}. Solid lines are linear fits to the data showing activated behaviour for limited regions of T and V_{bg} (charge density). **c**, The dependence of μ on T shows a pronounced low-temperature regime consistent with transport dominated by scattering from charged impurities. Above ~200 K, μ is limited by phonon scattering and follows a $\mu \sim T^{-1.4}$ dependence. Error bars are estimated on the basis of uncertainties in determining the voltage drop across the channel.

as the temperature is decreased, whereas for higher gate voltages, corresponding to charge densities above $n_{2D} \sim 1 \times 10^{13}$ cm^{-2}, the conductance increases as the temperature is decreased, which is the hallmark of metallic behaviour. In the inset of Fig. 3a are shown double sweeps of I_{ds}–V_{ds} characteristics for several temperatures at $V_{tg} = 0$ V with negligible hysteresis for all temperatures, excluding the possibility of hysteresis influencing our conclusions related to MIT. Fig. 3b shows the temperature dependence of the device conductance for different values of the charge density n_{2D}. We can see here more clearly that above the critical charge density of 1×10^{13} cm^{-2}, the conductance of monolayer MoS_2 increases with decreasing temperature, which is the manifestation of metallic behaviour. For charge densities smaller than 1×10^{13} cm^{-2}, the conductance decreases with the temperature, corresponding to semiconducting behaviour. This striking feature occurs when the conductivity is of the order of the quantum conductance e^2/h, the minimum of metallic conductivity, which was considered not to exist in 2D electronic systems according to the scaling theory of localization based on non-interacting electronic gases proposed in 1979[33].

The first step in our analysis is to define the critical point of the MIT. Inspecting Fig. 3a, we can see that each two consecutive isotherms of $G(V_{tg})$ cross each other at some value of V_{tg}. These intersections are temperature dependent, so an unambiguous determination of the transition is not possible. Fortunately, at temperatures under 80 K, the crossing point seems to be independent of the temperature and emerges at a well-defined point $V_{tg} = 2.2$ V, clearly separating the metallic and insulating phases. This transition point is the direct consequence of quantum interference effects of weak and strong localization. At lower carrier concentrations ($< n_{2D} \sim 1 \times 10^{13}$ cm^{-2}) the system is in the insulating state and strong localization[34] prevails. This charge density is comparable to that recorded for 20-nm-thick MoS_2 (ref. 13). As the top-gate bias is increased above $V_{tg} = 2.2$ V (concentration above $n_{2D} \sim 1 \times 10^{13}$ cm^{-2}), the system is driven into a metallic phase and weak localization seems to be the dominant effect. The observed quantum critical point of MIT in our devices is the consequence of a strongly correlated 2D electron gas[35]. As the system is confined in two dimensions, strong Coulomb interactions between electrons could cause a large ratio[36] r_s between potential (Coulomb, E_C) and kinetic (Fermi, E_F) energy:

$$r_s = \frac{E_C}{E_F} = \frac{n_v}{a_B^* \sqrt{\pi n_{2D}}} = \frac{n_v m^* e^2}{4\pi\varepsilon\hbar^2 \sqrt{\pi n_{2D}}}$$

where n_v is the number of degenerate valleys in the spectrum, $a_B^* = (4\pi\varepsilon\hbar^2)/(m^* e^2)$ is the effective Bohr radius, with ε being the dielectric constant and m^* is the effective electron mass. A system with $r_s \gg 1$ cannot be considered as non-interacting and the conclusion of scaling theory of localization[33] is not valid in this regime. In the case of monolayer MoS_2 we obtain $r_s \approx 4.2$, considering $m^* = 0.45 m_o$ (ref. 22), $\varepsilon = 7.3\varepsilon_o$ (ref. 37), a double-degenerate conduction band around the K point ($n_v = 2$) and an electron concentration at the transition of $n_{2D} \sim 1 \times 10^{13}$ cm^{-2}. This value is similar to those previously measured in the case of GaAs/AlGaAs heterostructures[38] ($r_s \sim 4$–5) and Si metal–oxide–semiconductor FETs[39] ($r_s \sim 8$). This shows that monolayer MoS_2 is a very attractive 2D system with strong Coulomb interactions, making the high-r_s regime easier to reach than in cleaner Si metal–oxide–semiconductor FETs or n-GaAs-based devices[40]. The reason for this is the relatively high effective mass (for Si: 0.19 m_o; n-GaAs: 0.07 m_o) and lower dielectric constant (for Si: 11.7 ε_o; n-GaAs: 12 ε_o) of monolayer MoS_2.

We can now also investigate the Ioffe–Regel criterion[41–43] for 2D semiconductors, which predicts the existence of a MIT when the parameter $k_F \cdot l_e$ satisfies the criterion $k_F \cdot l_e \sim 1$, with the Fermi wave vector $k_F = \sqrt{2\pi n_{2D}}$, and mean free path of electrons $l_e = \hbar k_F \sigma / n_{2D} e^2$. According to this criterion, for $k_F \cdot l_e \gg 1$ the phase is metallic whereas for $k_F \cdot l_e \ll 1$, the phase is insulating. For our device, at the crossing point of $V_{tg} = 2.2$ V, we have $k_F \cdot l_e \sim 2.5$, in good agreement with the theory. Our other devices also exhibit $k_F \cdot l_e$ close to 2 (Supplementary Table S1).

The temperature dependence of the mobility is extracted from conductance curves in the $V_{tg} = 1$–5 V range, using the expression

© 2013 Macmillan Publishers Limited. All rights reserved.

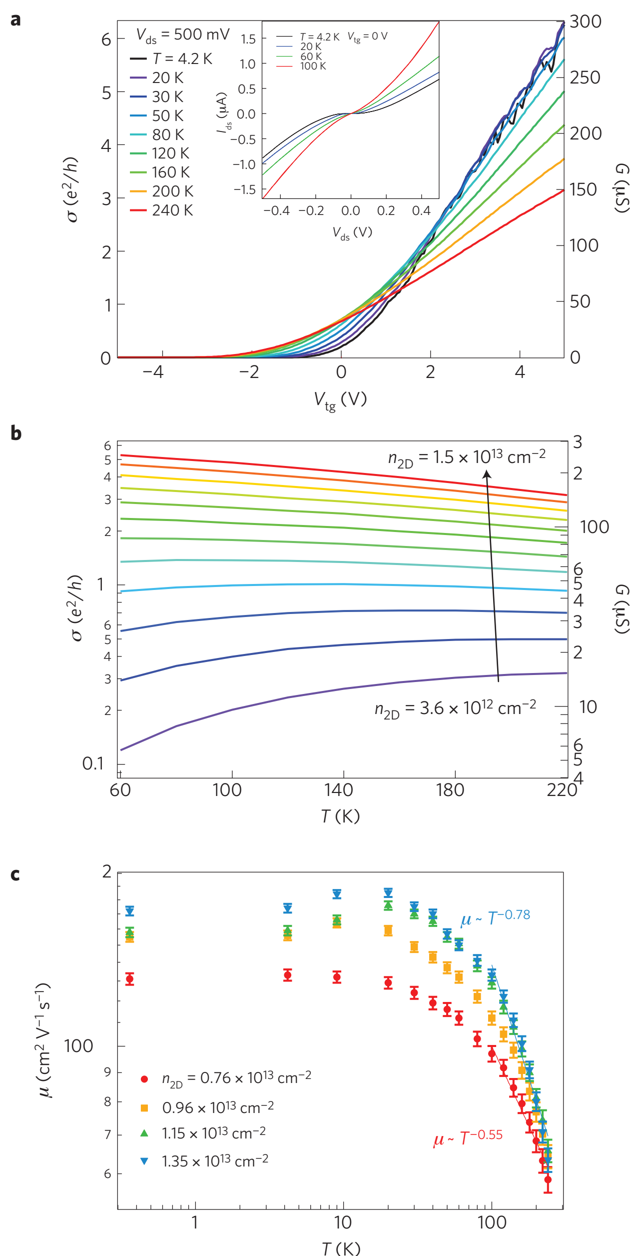

Figure 3 | Electron transport in dual-gated monolayer MoS_2. a, G and σ for different values of V_{tg} and T. For low values of V_{tg}, σ decreases with T. Above $V_{tg} \sim$1–2 V, monolayer MoS_2 enters a metallic state, with increasing σ as T is decreased. The inset shows double I_{ds}–V_{ds} sweeps. **b**, T-dependence of σ for different values of n_{2D}. **c**, μ is practically independent of T under 30 K, indicating screening of charged impurities due to deposition of the top-gate dielectric. Above ~100 K, μ decreases owing to phonon scattering and follows a $T^{-\gamma}$ dependence with $\gamma = 0.55$–0.78. The strongly reduced value of the exponent γ with respect to the single-gated device ($\gamma = 1.4$) is indicative of phonon mode quenching. Error bars are estimated on the basis of uncertainties in determining the voltage drop across the channel.

for field-effect mobility $\mu = [dG/dV_{bg}] \times [L_{12}/(WC_{tg,Hall})]$, with capacitance $C_{tg,Hall}$ extracted from Hall-effect measurements. For all dual-gate devices that we have characterized, we observe a monotonous increase of the mobility as the temperature is decreased with a saturation at low temperatures. Figure 3c shows the temperature dependence of mobility for the main device presented here. The mobility at 4 K is 174 cm^2 V s^{-1}, reaching 63 cm^2 V s^{-1} at 240 K for $n_{2D} \sim 1.35 \times 10^{13}$ cm^{-2}. This is a distinct difference from devices fabricated in a single-gate configuration (Fig. 2c). We relate this behaviour to effective damping of Coulomb scattering on charged impurities due to the presence of the high-κ dielectric and the metallic top gate that changes the dielectric environment of monolayer MoS_2 (ref. 27). At low temperatures, the influence of charged impurities on mobility is stronger for lower electron densities. For example, at 10 K for $n_{2D} \sim 0.76 \times 10^{13}$ cm^{-2} we extracted a mobility of 132 cm^2 V s^{-1} whereas for $n_{2D} \sim 1.35 \times 10^{13}$ cm^{-2} we extracted a mobility of 184 cm^2 V s^{-1}. In the phonon-limited part between 100 and 300 K, the mobility can be fitted to the expression $\mu \sim T^{-\gamma}$, with the exponent γ being in the 0.55–0.78 range for electron concentrations n_{2D} between $\sim 0.76 \times 10^{13}$ cm^{-2} and 1.35×10^{13} cm^{-2} (Fig. 3c). For all of our double-gated monolayer devices we find this exponent to be between 0.3 and 0.78, whereas for one double-layer device we find a value of 1.47. These values for monolayer MoS_2 are much smaller than the theoretically predicted value of $\gamma \approx 1.52$ (ref. 30) or bulk crystals ($\gamma \approx 2.6$; ref. 24). This indicates that in addition to the quenching of the homopolar phonon mode, other mechanisms might influence the mobility of monolayer MoS_2 in dual-gated devices, for example, phonon screening induced by the metallic top gate or a change in the strength of electron–phonon coupling. Further theoretical modelling could shed more light on these mechanisms.

Just as in the case of single-gated devices, we model the temperature dependence of G in the insulating regime of our double-gated devices with thermally activated behaviour (Fig. 4a). Here, we observe that the activated behaviour fits our data very well in the 100–250 K temperature range, with extracted activation energies E_a shown in Fig. 4b.

We have performed Hall-effect measurements on all MoS_2 devices covered with a dielectric layer presented here to accurately determine the mobility, density of charge carriers and the capacitive coupling of MoS_2 layers to control gate electrodes (bottom or top gates). Figure 5a shows the transverse Hall resistance R_{xy} of our main dual-gated monolayer device, which follows a linear dependence on the magnetic field B. From the inverse slope of R_{xy} we can directly determine the electron density n_{2D} in the MoS_2 channel. The variation of the electron density extracted from R_{xy} as a function of the top-gate voltage V_{tg} is shown in Fig. 5b. The slope of this dependence gives directly the capacitance $C_{tg,Hall} = 3.17 \times 10^{-7}$ F cm^{-2} used in calculation of the field-effect mobility (Fig. 3c). We also directly measure the capacitive coupling between the channel and the bottom gate in devices where the MoS_2 channel is covered with a dielectric layer and in devices with disconnected top gates and compare them with the geometric capacitance per unit area calculated using the parallel-plate capacitance model $C_{geom} = \varepsilon_0\varepsilon_r/d_{ox,bottom}$, where $d_{ox,bottom}$ is the thickness of the bottom-gate oxide[10]. We find that encapsulation in a dielectric can increase the capacitive coupling from C_{geom} by a factor of 2.4, similarly to graphene devices[45], and disconnecting the top gate increases the capacitive coupling by a factor of 53 (Supplementary Fig. S4). These measurements prove that the capacitance can be underestimated in a complicated dielectric environment, both in the case of disconnected top gates[10–12] and encapsulation[44,46], resulting in mobility values that are probably overestimated. To accurately measure the field-effect mobility of FETs based on 2D materials one needs to measure the actual capacitance using either cyclic voltammetry[28] or Hall-effect measurements as outlined here.

In conclusion, we have performed conductance and mobility measurements on monolayer MoS_2 FETs in single- and dual-gate configurations. Using a top gate and solid-state dielectrics, we were able to tune the charge carrier density to more than $n_{2D} \sim 3.6 \times 10^{13}$ cm^{-2}, inducing the transition from the insulating to the metallic phase in monolayer MoS_2. A quantum critical point, separating the metallic phase, stabilized by electronic interactions,

© 2013 Macmillan Publishers Limited. All rights reserved.

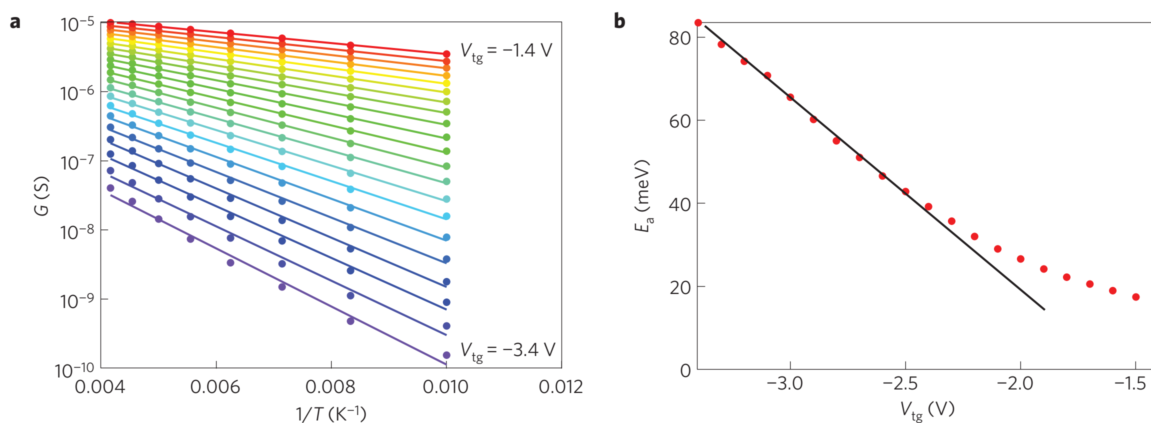

Figure 4 | E_a for the top-gated monolayer MoS_2 in the insulating regime. a, Arrhenius plot of the conductance of monolayer MoS_2 covered with HfO_2, in the insulating regime. **b**, Dependence of E_a on V_{tg}.

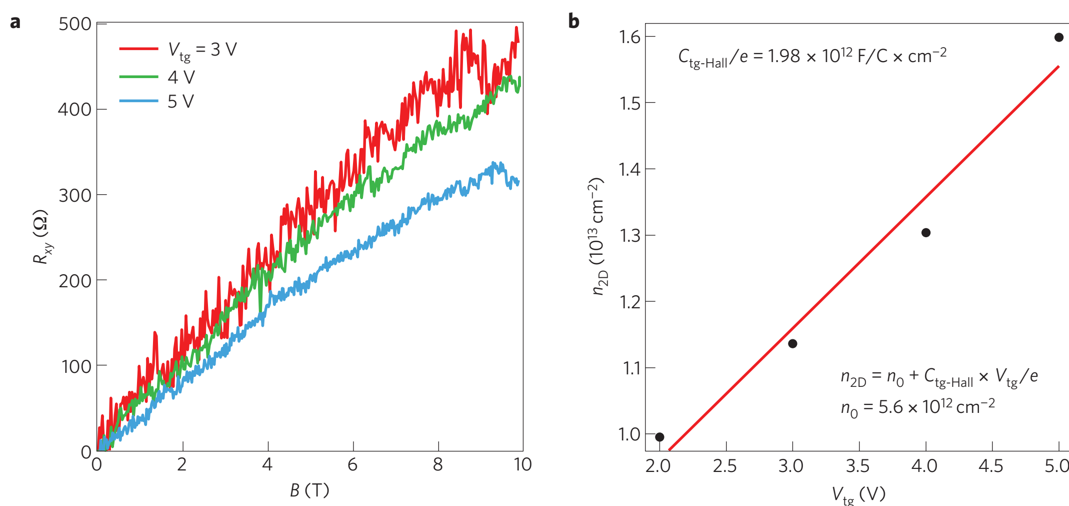

Figure 5 | Hall-effect measurements in the dual-gated monolayer MoS_2 device. a, Hall resistance R_{xy} versus B for different positive values of V_{tg}. **b**, Electron concentration n_{2D} extracted from R_{xy} or different values of V_{tg}. From the slope of the red solid line we calculate the capacitance per unit area $C_{tg,Hall}$ of the top-gate MoS_2 device. The residual doping of the MoS_2 channel is $n_o = 5.6 \times 10^{12}$ cm^{-2}. All measurements are performed at $T = 4$ K with a grounded back-gate electrode.

from the insulating phase, where disorder prevails over the electronic interactions, has been identified. This transition point is in good agreement with theory and shows that monolayer MoS_2 could be an interesting new material system for investigating low-dimensional correlated electron behaviour. The MIT could also be used for new types of switch, especially fast optoelectronic switches based on differences in optical transmission in metallic and insulating states[47]. In addition to allowing high charge densities, the high-κ HfO_2 used as the top-gate dielectric also changes the dielectric environment and effectively screens Coulomb scattering, which results in mobility improvement in dual-gate devices. Furthermore, the presence of the top-gate dielectric and metal electrode results in a quenching of the homopolar mode, which is polarized in the direction normal to the layer, leading to a strong decrease of the mobility exponent γ in $\mu \sim T^{-\gamma}$. Our results provide a new picture of the mobility issue in different configurations of MoS_2 devices, which should shed new light on the directions for further improvements in device quality and characterization techniques.

Methods

MoS_2 flakes were exfoliated from molybdenite crystals (SPI Supplies Brand Moly Disulphide) by the Scotch-tape micromechanical cleavage technique. ALD was performed in a Beneq system using the reaction of H_2O with tetrakis(ethyl-methylamido)hafnium. Electrical characterization was carried out using National Instruments DAQ cards, SR570 current preamplifiers, SR560 low noise voltage preamplifiers, and an Oxford Instruments Heliox cryo-magnetic system.

Received 11 January 2013; accepted 15 May 2013; published online 23 June 2013

References

1. Wang, Q. H., Kalantar-Zadeh, K., Kis, A., Coleman, J. N. & Strano, M. S. Electronics and optoelectronics of two-dimensional transition metal dichalcogenides. *Nature Nanotech.* **7,** 699–712 (2012).
2. Novoselov, K. S. *et al.* Two-dimensional atomic crystals. *Proc. Natl Acad. Sci. USA* **102,** 10451–10453 (2005).
3. Coleman, J. N. *et al.* Two-dimensional nanosheets produced by liquid exfoliation of layered materials. *Science* **331,** 568–571 (2011).
4. Smith, R. J. *et al.* Large-scale exfoliation of inorganic layered compounds in aqueous surfactant solutions. *Adv. Mater.* **23,** 3944–3948 (2011).
5. Liu, K-K. *et al.* Growth of large-area and highly crystalline MoS_2 thin layers on insulating substrates. *Nano Lett.* **12,** 1538–1544 (2012).
6. Zhan, Y., Liu, Z., Najmaei, S., Ajayan, P. M. & Lou, J. Large-area vapor-phase growth and characterization of MoS_2 atomic layers on a SiO_2 substrate. *Small* **8,** 966–971 (2012).
7. Bertolazzi, S., Brivio, J. & Kis, A. Stretching and breaking of ultrathin MoS_2. *ACS Nano.* **5,** 9703–9709 (2011).

© 2013 Macmillan Publishers Limited. All rights reserved.

8. Brivio, J., Alexander, D. T. L. & Kis, A. Ripples and layers in ultrathin MoS_2 membranes. *Nano Lett.* **11,** 5148–5153 (2011).
9. Lembke, D. & Kis, A. Breakdown of high-performance monolayer MoS_2 transistors. *ACS Nano.* **6,** 10070–10075 (2012).
10. Radisavljevic, B., Radenovic, A., Brivio, J., Giacometti, V. & Kis, A. Single-layer MoS_2 transistors. *Nature Nanotech.* **6,** 147–150 (2011).
11. Radisavljevic, B., Whitwick, M. B. & Kis, A. Integrated circuits and logic operations based on single-layer MoS_2. *ACS Nano.* **5,** 9934–9938 (2011).
12. Radisavljevic, B., Whitwick, M. B. & Kis, A. Small-signal amplifier based on single-layer MoS_2. *Appl. Phys. Lett.* **101,** 043103 (2012).
13. Ye, J. T. *et al.* Superconducting dome in a gate-tuned band insulator. *Science* **338,** 1193–1196 (2012).
14. Lebegue, S. & Eriksson, O. Electronic structure of two-dimensional crystals from *ab initio* theory. *Phys. Rev. B* **79,** 115409 (2009).
15. Kuc, A., Zibouche, N. & Heine, T. Influence of quantum confinement on the electronic structure of the transition metal sulfide TS_2. *Phys. Rev. B* **83,** 245213 (2011).
16. Splendiani, A. *et al.* Emerging photoluminescence in monolayer MoS_2. *Nano Lett.* **10,** 1271–1275 (2010).
17. Mak, K. F., Lee, C., Hone, J., Shan, J. & Heinz, T. F. Atomically thin MoS_2: A new direct-gap semiconductor. *Phys. Rev. Lett.* **105,** 136805 (2010).
18. Mak, K. F., He, K., Shan, J. & Heinz, T. F. Control of valley polarization in monolayer MoS_2 by optical helicity. *Nature Nanotech.* **7,** 494–498 (2012).
19. Zeng, H., Dai, J., Yao, W., Xiao, D. & Cui, X. Valley polarization in MoS_2 monolayers by optical pumping. *Nature Nanotech.* **7,** 490–493 (2012).
20. Cao, T. *et al.* Valley-selective circular dichroism of monolayer molybdenum disulphide. *Nature Commun.* **3,** 887 (2012).
21. Feng, W. *et al.* Intrinsic spin Hall effect in monolayers of group-VI dichalcogenides: A first-principles study. *Phys. Rev. B* **86,** 165108 (2012).
22. Yoon, Y., Ganapathi, K. & Salahuddin, S. How good can monolayer MoS_2 transistors be? *Nano Lett.* **11,** 3768–3773 (2011).
23. Alam, K. & Lake, R. K. Monolayer MoS_2 transistors beyond the technology road map. *Elect. Dev. IEEE Trans.* **59,** 3250–3254 (2012).
24. Fivaz, R. & Mooser, E. Mobility of charge carriers in semiconducting layer structures. *Phys. Rev.* **163,** 743–755 (1967).
25. Ghatak, S., Pal, A. N. & Ghosh, A. Nature of electronic states in atomically thin MoS_2 field-effect transistors. *ACS Nano.* **5,** 7707–7712 (2011).
26. Jena, D. & Konar, A. Enhancement of carrier mobility in semiconductor nanostructures by dielectric engineering. *Phys. Rev. Lett.* **98,** 136805 (2007).
27. Han, L. & Ye, P. D. MoS_2 dual-gate MOSFET with atomic-layer-deposited Al_2O_3 as top-gate dielectric. *Elect. Dev. Lett. IEEE* **33,** 546–548 (2012).
28. Kim, S. *et al.* High-mobility and low-power thin-film transistors based on multilayer MoS_2 crystals. *Nature Commun.* **3,** 1011 (2012).
29. Ming-Wei, L. *et al.* Mobility enhancement and highly efficient gating of monolayer MoS_2 transistors with polymer electrolyte. *J. Phys. D* **45,** 345102 (2012).
30. Kaasbjerg, K., Thygesen, K. S. & Jacobsen, K. W. Phonon-limited mobility in n-type single-layer MoS_2 from first principles. *Phys. Rev. B* **85,** 115317 (2012).
31. Sze, S. M. & Ng, K. K. *Physics of Semiconductor Devices* (Wiley, 2007).
32. Mott, N. F. *Metal-Insulator Transitions* (Barnes Noble Books, Taylor Francis, 1974).
33. Abrahams, E., Anderson, P. W., Licciardello, D. C. & Ramakrishnan, T. V. Scaling theory of localization: Absence of quantum diffusion in two dimensions. *Phys. Rev. Lett.* **42,** 673–676 (1979).
34. Evers, F. & Mirlin, A. D. Anderson transitions. *Rev. Mod. Phys.* **80,** 1355–1417 (2008).
35. Punnoose, A. & Finkel'stein, A. M. Metal-insulator transition in disordered two-dimensional electron systems. *Science* **310,** 289–291 (2005).
36. Ho, L. H., Micolich, A. P., Hamilton, A. R. & Sushkov, O. P. Ground-plane screening of Coulomb interactions in two-dimensional systems: How effectively can one two-dimensional system screen interactions in another. *Phys. Rev. B* **80,** 155412 (2009).
37. Salmani-Jelodar, M., Yaohua, T. & Klimeck, G. Single layer MoS_2 band structure and transport. *Proc. Int. Semiconductor Device Research Symp.* (ISDRS) 1–2 (2011).
38. Ghosh, A. *et al.* Electron assisted variable range hopping in strongly correlated 2D electron systems. *Phys. Status Solidi B* **230,** 211–216 (2002).
39. Okamoto, T., Hosoya, K., Kawaji, S. & Yagi, A. Spin degree of freedom in a two-dimensional electron liquid. *Phys. Rev. Lett.* **82,** 3875–3878 (1999).
40. Dobrosavljevic, V., Trivedi, N. & Valles, J. M. *Conductor-Insulator Quantum Phase Transitions* (Oxford Univ. Press, 2012).
41. Gurvitch, M. Ioffe-Regel criterion and resistivity of metals. *Phys. Rev. B* **24,** 7404–7407 (1981).
42. Mark, R. G., Adkins, C. J., Haim, B. & Ralph, R. Experimental study of the Ioffe-Regel criterion for amorphous indium oxide films. *J. Phys. Condens. Matter* **10,** 809–819 (1998).
43. Lee, P. A. & Ramakrishnan, T. V. Disordered electronic systems. *Rev. Mod. Phys.* **57,** 287–337 (1985).
44. Das, S., Chen, H-Y., Penumatcha, A. V. & Appenzeller, J. High performance multilayer MoS_2 transistors with scandium contacts. *Nano Lett.* (2012).
45. Xia, J. L., Chen, F., Wiktor, P., Ferry, D. K. & Tao, N. J. Effect of top dielectric medium on gate capacitance of graphene field effect transistors: Implications in mobility measurements and sensor applications. *Nano Lett.* **10,** 5060–5064 (2010).
46. Bao, W., Cai, X., Kim, D., Sridhara, K. & Fuhrer, M. S. High mobility ambipolar MoS_2 field-effect transistors: substrate and dielectric effects. *Appl. Phys. Lett.* **102,** 042104 (2013).
47. Chudnovskiy, F., Luryi, S. & Spivak, B. in *Future Trends in Microelectronics: The Nano Millennium* (eds Luriy, S., Xu, J.M. & Zaslavsky, A.) Part II, 148–155 (Wiley, 2002).

Acknowledgements

We thank W. Escoffier (LNCMI CNRS), B. Raquet (LNCMI CNRS) and S. Bertolazzi (EPFL) for useful discussions as well as J-S. Heron (EPFL) for technical support. Device fabrication was carried out in part in the EPFL Center for Micro/Nanotechnology (CMI). We thank Z. Benes (CMI) for technical support with electron-beam lithography and A. Radenovic and M. Whitwick (EPFL) for support with ALD deposition. This work was financially supported by ERC grant no. 240076, FLATRONICS: Electronic devices based on nanolayers.

Author contributions

B.R. worked on device fabrication and performed the measurements. A.K. designed the experiment and initiated the research. B.R. and A.K. analysed the results and wrote the manuscript.

Additional information

Supplementary information is available in the online version of the paper. Reprints and permissions information is available online at www.nature.com/reprints. Correspondence and requests for materials should be addressed to A.K.

Competing financial interests

The authors declare no competing financial interests.

© 2013 Macmillan Publishers Limited. All rights reserved.